Check for updates

RESEARCH ARTICLE

ADVANCED ELECTRONIC MATERIALS
www.advelectronicmat.de

Temperature of Conductive Nanofilaments in Hexagonal Boron Nitride Based Memristors Showing Threshold Resistive Switching

Mario Lanza, Felix Palumbo,* Yuanyuan Shi, Fernando Aguirre, Santiago Boyeras, Bin Yuan, Eilam Yalon, Enrique Moreno, Tianru Wu, and Juan B. Roldan*

Two-terminal metal/insulator/metal (MIM) memristors exhibiting threshold resistive switching (RS) can develop advanced key tasks in solid-state nano/micro-electronic circuits, such as selectors and integrate-and-fire electronic neurons. MIM-like memristors using multilayer hexagonal boron nitride (h-BN) as dielectric are especially interesting because they have shown threshold RS with ultra-low energy consumption per state transition down to the zeptojoule regime. However, the factors enabling stable threshold RS at such low operation energies are still not fully understood. Here it is shown that the threshold RS in 150 nm × 150 nm Au/Ag/h-BN/Au memristors is especially stable because the temperature in the h-BN stack during operation (i.e., at low currents ≈1 µA) is very low (i.e., ≈310 K), due to the high in-plane thermal conductivity of h-BN and its low thickness. Only when the device is operated at higher currents (i.e., ≈200 µA) the temperatures at the h-BN increase remarkably (i.e., >500 K), which produce a stable non-volatile conductive nanofilament (CNF). This work can bring new insights to understand the performance of 2D materials based RS devices, and help to develop the integration of 2D materials in high-density nanoelectronics.

1. Introduction

Two-terminal threshold-type resistive switching (RS) devices with a metal/insulator/metal (MIM) structure are attractive solid-state microelectronic devices for massive parallel information processing and storage, and they have been recently used as integrate-and-fire neurons in spiking neural networks.[1–2] In most MIM-like RS devices the application of electrical stresses between the electrodes results in a progressive increase of the conductance,[3] which is a non-volatile phenomenon (i.e., the changes in the conductance remain stable after the bias is removed). This phenomenon is related to the formation of defects in the microstructure of the insulator, which can be related to the movement of intrinsic species (i.e., oxygen ions in transition metal oxides [TMO]), or penetration of metallic ions from the electrodes into the insulator.[4] If the electrical

M. Lanza
Physical Sciences and Engineering Division
King Abdullah University of Science and Technology (KAUST)
Thuwal 23955–6900, Saudi Arabia
E-mail: mario.lanza@kaust.edu.sa

F. Palumbo, F. Aguirre, S. Boyeras
Unidad de Investigación y Desarrollo de las Ingenierías-CONICET
Facultad Regional, Buenos Aire
Universidad Tecnológica Nacional
(UIDI-CONICET/FRBA-UTN)
Medrano 951, Buenos Aires C1179AAQ, Argentina
E-mail: felix.palumbo@conicet.gov.ar

Y. Shi
IMEC
Kapeldreef 75, Leuven 3001, Belgium

B. Yuan
Department of Electronic and Biomedical Engineering
Universitat de Barcelona
Martí i Franquès 1
Barcelona E-08028, Spain

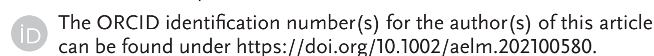
The ORCID identification number(s) for the author(s) of this article can be found under https://doi.org/10.1002/aelm.202100580.

DOI: 10.1002/aelm.202100580

B. Yuan
Materials Science and Engineering Department
Guangdong Technion – Israel Institute of Technology
Shantou 515063, China

E. Yalon
Andrew and Erna Viterbi Faculty of Electrical Engineering
Technion–Israel Institute of Technology
Haifa 32000, Israel

E. Moreno
UJM-Saint-Etienne
CNRS
Institute of Optics Graduate School
University of Lyon
Laboratoire Hubert Curien
UMR5516, St-Etienne F-42023, France

T. Wu
School of Physical Science and Technology
Shanghai Tech University
393 Middle Huaxia Road, Shanghai, Pudong 201210, China

J. B. Roldan
Departamento de Electrónica y Tecnología de Computadores
Facultad de Ciencias
Universidad de Granada
Avd. Fuentenueva s/n, Granada 18071, Spain

 © 2021 Wiley-VCH GmbH

stresses applied are severe enough, these ions can form one/few effective conductive nano-filaments (CNF) that connect both electrodes, which triggers the dielectric breakdown (BD) of the insulator. In non-volatile MIM-like RS devices, this CNF can be disrupted, either by atomic diffusion[5–7] or thermal effects,[8–9] when additional electrical stresses are applied, which are referred as unipolar RS or bipolar RS if the polarity of this additional stress is the same or opposed to that used to trigger the BD (respectively).[10] However, when using some specific metallic electrodes and insulating materials, the conductance increase is volatile (i.e., the initial conductance is self-recovered when the bias is removed).[3] This phenomenon, which can take place either before or after triggering the BD, is referred as threshold-type RS.

Recent studies have reported that MIM-like RS devices using Ag electrodes show outstanding threshold-type RS, due to the high diffusivity of Ag^+ ions into different types of insulators (including SiO_X, HfO_X, and MgO_X).[11] Recently, it has been discovered that the combination of Ag electrodes and multilayer hexagonal boron nitride (h-BN) insulating films grown by chemical vapor deposition (CVD) results in threshold-type RS with ultra-low energy consumption (≈8.8 zJ)[12] —note that this is the lowest energy consumption ever reported for any type of RS device, which is very close to the fundamental limit of the thermal noise (≈4.1 zJ).[13] Moreover, metal/h-BN/metal devices exhibit coexistence of both non-volatile (i.e., bipolar) and volatile (i.e., threshold-type) RS,[14] which allows their use as electronic synapses to emulate both long-term plasticity (LTP) and short-term plasticity (STP).[15] It is believed that the observation of both RS regimes in the same MIM cell is related to the lateral size of the CNF triggered during the BD,[15] which can be controlled by limiting the energy delivered during the BD, either using low current compliances (I_{CC}) or a series resistor/transistor during ramped voltage stresses (RVS), or applying low voltage and/or short times during pulsed voltage stresses (PVS).

Despite these advances, the key factors allowing metal/h-BN/metal devices to exhibit threshold-type RS are still not fully understood. Here we show that Ag/h-BN/Au devices can be operated reliably in the threshold-RS regime because the CNF temperature is kept low enough (i.e., ≈310 K), and that a stable non-volatile regime is reached when the temperature of the CNF increases remarkably (i.e., >500 K). All the methods we used for the fabrication of the devices are scalable, the size of the devices studied is 150 nm × 150 nm, and all the conclusions are demonstrated statistically in 58 devices. Our work provides essential knowledge to understand the performance and reliability of h-BN based RS devices and paves the way for their introduction in high-density industrial wafers.

2. Results and Discussion

2.1. Performance of Metal/h-BN/Metal Nano-Memristors

h-BN sheets with thicknesses of ≈4 layers are synthesized by CVD and used to fabricate 150 nm × 150 nm Ag/h-BN/Au devices, with the assistance of electron beam lithography and electron beam evaporation (see the Experimental Section). **Figure 1**a shows a representative cross-sectional transmission electron microscopy (TEM) image of the as-grown h-BN stacks, and Figure 1b shows a representative scanning electron microscopy (SEM) image of the Ag/h-BN/Au devices. The presence of RS in these devices is first analyzed by applying sequences of RVS with different I_{CC}, and constructing current versus voltage (I–V) plots. When using an I_{CC} low enough (i.e., 1 µA), the I–V plots reveal stable threshold-type RS, and the set and reset transitions can be clearly observed (see Figure 1c). When using an I_{CC} high enough (i.e., 1 mA), the I–V plots reveal non-volatile BD (see Figure 1d), which is demonstrated by the absence of a reset transition. In this regime, the CNF has been completely formed, as confirmed by the linear conduction observed when plotting the data in linear scale (see inset in Figure 1d). In our previous studies,[14–15] we demonstrated that the formation of CNFs across multilayer h-BN is related to the penetration of metallic ions from the adjacent electrodes when an electrical stress is applied, a phenomenon that is favored by the formation of boron vacancies. When using moderate I_{CC} (i.e., between 1 µA and 1 mA), the devices exhibit unstable volatile RS, i.e., the self-disruption of the CNF fluctuates between few milliseconds to tens of seconds. Our experiments indicate that the maximum I_{CC} that allows stable threshold-type RS and the minimum I_{CC} that produces non-volatile BD are slightly different for each device, and we conclude that for a population of 58 devices, threshold-RS always occurs for $I_{CC} < 10$ µA, and non-volatile BD always occurs for $I_{CC} > 200$ µA (see bluish regions in Figure 1c,d). It should be noted that these I_{CC} values apply for the Ag/h-BN/Au devices analyzed in this study, and that for thicker h-BN or different electrode materials, stable threshold RS at higher I_{CC} (up to ≈100 µA) has been also observed.[14] The switching voltages (V_{SET} and V_{RESET}) also slightly change from one device-to-another (as expected),[12] probably due to local fluctuations of the thickness and density of defects in the h-BN stack.

We study the dynamic response of the Ag/h-BN/Au devices in depth by applying sequences of PVS with different amplitudes, matching the real working conditions of electronic synapses and neurons in an SNN,[16] and we record the currents driven simultaneously. In each test, we apply write PVS with a constant amplitude (V_W, which was set to 2, 2.5, 3, 3.5, and 4 V during different tests) aimed to modify the conductance of the Ag/h-BN/Au devices, and after each write PVS we intercalated read pulses with an amplitude (V_R) of 0.1 V. The duration of the write pulse (T_W) and read pulse (T_R) was 2 ms, and between all the pulses the voltage (V_{DOWN}) was kept to 0 V during 2 ms (T_{DOWN}). As an example, **Figure 2**a,b shows the current signal driven by the Ag/h-BN/Au devices when applying PVS with V_W = 2 V and V_W = 4 V, respectively. During T_{DOWN} the current fluctuates at ≈1 nA, which is the noise level of the semiconductor parameter analyzer (SPA) for this current range of operation, it is similar to that in ref. [17]. The current across the device increases gradually during T_W until reaching an almost constant level (I_{SET}), which depends on the value of V_W (see point 3 in Figure 2c). For each value of V_W, I_{SET} shows certain variability, but the overall increasing trend of I_{SET} with V_W is very clear (see Figure 2e). After each write pulse the currents go back to ≈1 nA, even during the following read pulse, indicating that the conductance of the Ag/h-BN/Au devices has been completely self-recovered. These conductivity changes should be related to the motion of Ag^+ ions into the h-BN stack during

© 2021 Wiley-VCH GmbH

ADVANCED ELECTRONIC MATERIALS
www.advelectronicmat.de

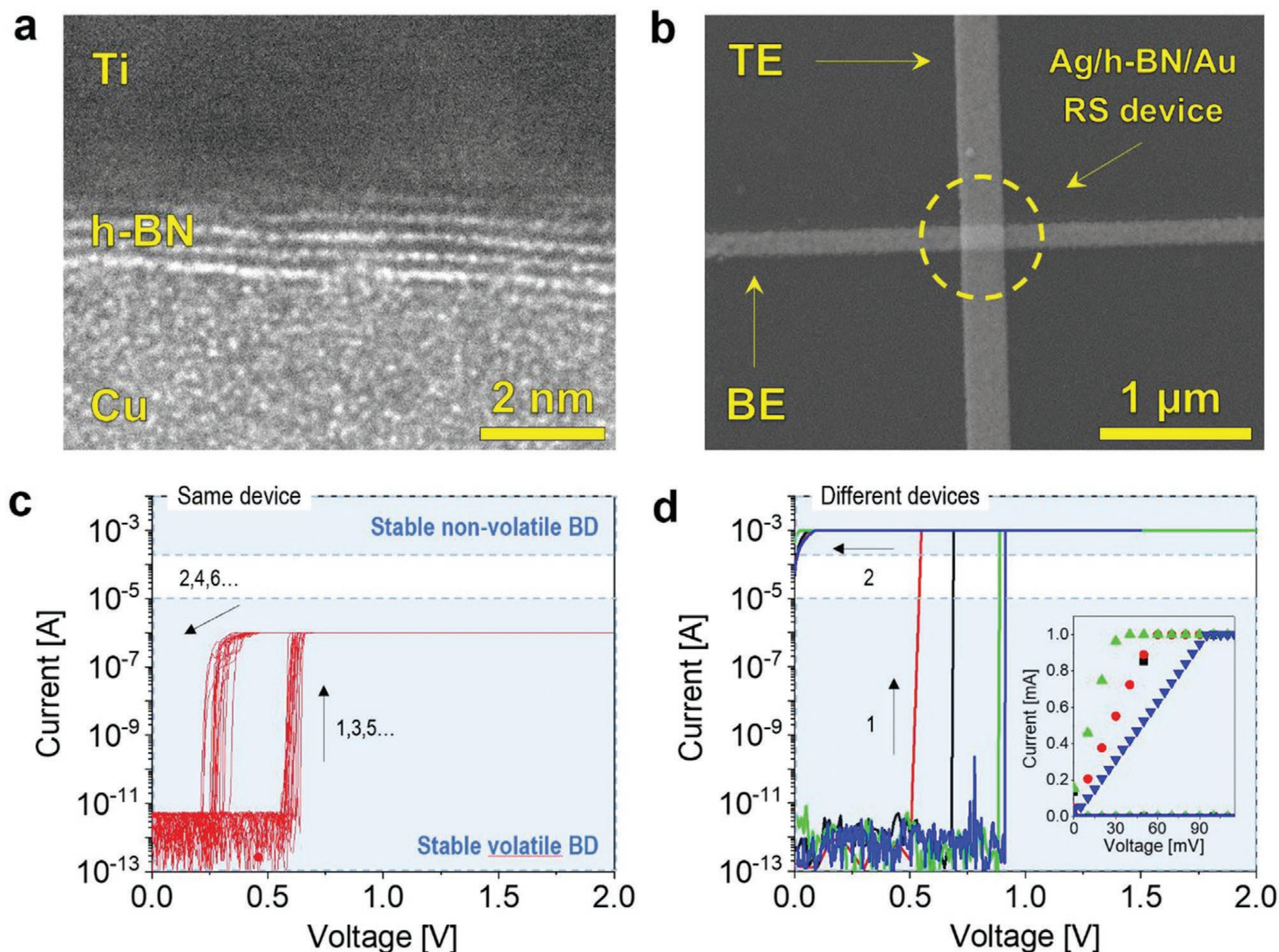

Figure 1. Structure and electrical performance of Ag/CVD-grown h-BN/Au device. a) Cross sectional TEM image of the as-grown CVD h-BN stacks on Cu foil, which is covered by Au/Ti thin films before the FIB fabrication. There are native defects existing in the as-grown h-BN stacks. b) SEM image of one Au/Ag/h-BN/Au structure based cross-point device. c) *I–V* plots showing bi-stable threshold-type RS cycles in one Au/Ag/CVD-grown h-BN/Au device at a current limitation of 1 µA. d) *I–V* plots showing non-volatile dielectric breakdown of different Au/Ag/CVD-grown h-BN/Au devices at a current limitation of 1 mA. The inset image is the current-voltage curves of (d) plotted in linear scale.

T_W, which may not reach a stable bonding state in the 2D layered h-BN stack and end up moving out during T_{DOWN} and T_R thanks to their high diffusivity.[11] This is supported by the fact that the application of similar PVS with opposed polarity does not show conductance relaxation, i.e., the Au^+ ions that penetrate in the h-BN stack do not have such high diffusivity and they stay inside the h-BN when the bias is removed, leading to non-volatile conductance changes. It is worth noting that complete relaxation after long sequences of PVS is an outstanding property that most MIM-based RS devices do not exhibit,[11,18–19] and should be related to the excellent mechanical and chemical stability of the 2D layered h-BN stack,[20–22] as well as to its high in-plane thermal conductivity.[23] We also detected one device that reached the non-volatile regime when using $V_W = 4$ V (see Figure 2b), which can be observed from the higher currents during V_W (which reach the saturation level of the SPA when operated in PVS mode, i.e., 100 µA) and the higher currents far above the noise level (≈2 µA) during V_R. If the value of V_W is further increased ≥4.5 V, most of the devices reach the non-volatile regime.

2.2. Temperature of the Nanofilament

The severity and reversibility of the BD event in ultra-thin dielectrics is closely related to the amount of energy transferred from the CNF to its surrounding atomic network.[24–25] This phenomenon depends on the CNF temperature, which at the same time depends on the current flowing across it—note that the current density can reach up to 10^8 A cm^{-2} as the size of the CNF is ≈50 nm^2 —,[26–28] and on the thermal conductivity of the dielectric and its surroundings. In order to obtain a simplified estimation of the temperature of the CNF in the h-BN stack using a single fitting parameter, it can be evaluated by using Equation (1):[24]

$$T = \frac{f_1 V I_{SET}}{2\pi t_{ox} \kappa} + T_{amb} \tag{1}$$

where T is the temperature, V is the applied voltage across the BD spot (i.e., V_W), I_{SET} is the current level at the onset of the synapse, t_{ox} is the dielectric thickness, k is the thermal

© 2021 Wiley-VCH GmbH

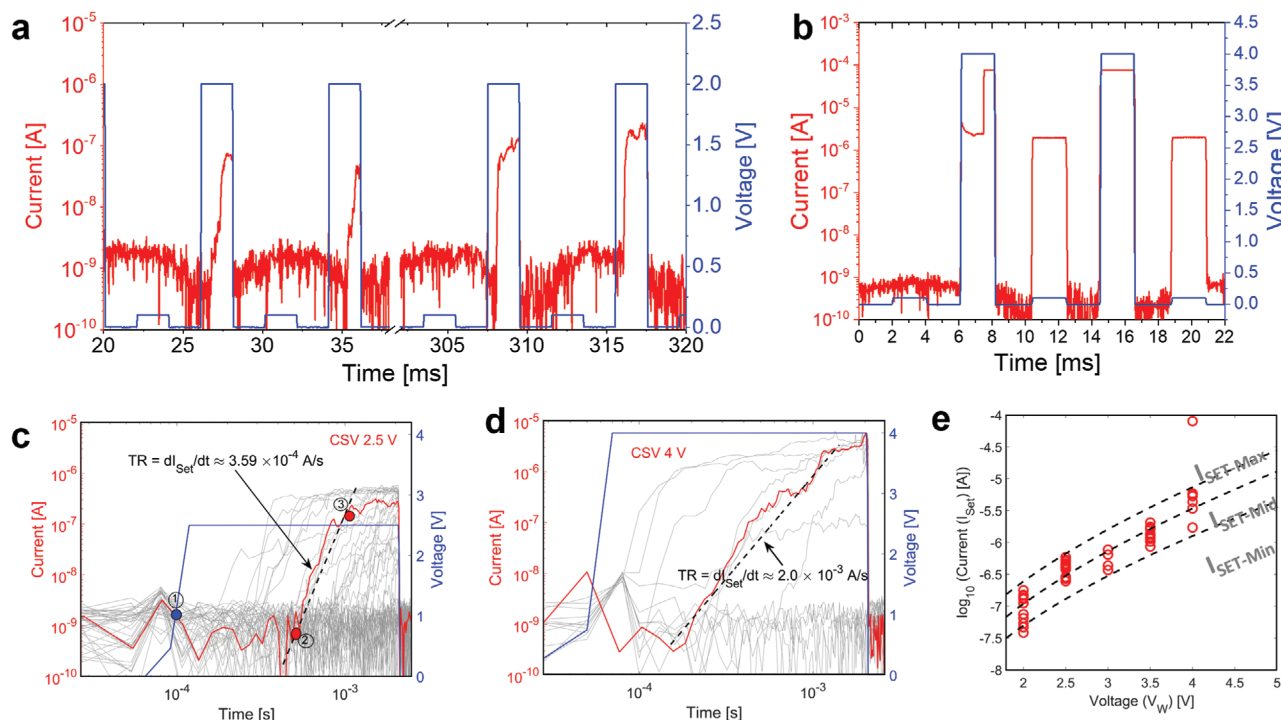

Figure 2. PVS measurement of the Au/Ag/CVD-grown h-BN/Au device at different pulse amplitudes. a) Experimental data acquired using a PVS with an amplitude of 2.5 V, shows a volatile switching. Current trace (red) shows the device transition from HRS to LRS when a voltage pulse (blue) is applied. This experiment is repeated for different pulse amplitudes, collecting between 20–30 transients for each amplitude. b) Experimental data acquired using a PVS with an amplitude of 4 V, shows a non-volatile switching. c,d) Current-time transients (grey and red) for PVS with a pulse amplitude of 2.5 and 4 V, respectively. The voltage waveforms are superimposed in both cases (blue traces). The transition between the high-resistance state and the low-resistance state is characterized in terms of the transition rate (slope of the current transient). A time-to-set is defined as the time between point 1 and point 2. A current plateau is observed after the device switches to the LRS. e) The post-SET current for each pulse transient as a function of the pulse amplitude.

conductivity of the dielectric, T_{amb} is the room temperature, and f_1 is a fitting parameter that is proportional to the power lost at the constriction (i.e., $I_{SET} \times V_W$). The values of I_{SET} and V_W are obtained from Figure 2d, and the value of f_1 chosen here is 0.1, in agreement with finite element simulations shown next, and with a previous report.[29] The solid lines in **Figure 3**a show the T as a function of I_{SET}, calculated using Equation (1). As it can be observed, for I_{SET} >100 µA the temperature starts to increase rapidly, reaching values close to the melting point of the materials (≈1000 K) in the regions where the CNF narrowing is located.

The values obtained using Equation (1) have been compared to those obtained by solving the 3D heat equation (Equation (2)) and the current equation for Ag/h-BN/Au structures.[30–31]

$$\nabla(k_{TH}(x,y,z)\nabla T(x,y,z)) + \dot{e}_{generated} = 0 \quad (2)$$

The steady-state heat equation was solved accounting for a specific current I_{SET} flowing through the CNF. The power density generated within the CNF was calculated in a point-to-point basis as σE^2, where σ stands for the local electrical conductivity and E for the local electric field.[32] The thermal time constant of the CNF is short compared with the duration of the applied pulses, and therefore the steady-state solution can be used.[33]

The simulation domain employed is shown in Figure 3b, the grid used was 0.13 nm, and the CNF was assumed to have a parabolic profile with a maximum radius of 5 nm at the Ag/h-BN interface and a minimum radius at the h-BN/Au interface, in agreement with previous observations.[14] The physical parameters used for the simulations are displayed in Table S1 (Supporting Information). We set the voltages to the values that generate currents of 1 and 200 µA, featuring the threshold-type and the non-volatile regimes (respectively). Our simulations (blue scattered points in Figure 3a) indicate that for a current of 1 µA the temperature of the CNF is below 310 K (Figure 3c), which is obviously insufficient to form a stable CNF and results in threshold-type RS (i.e., volatile BD). On the contrary, for a current of 200 µA the temperature rises above ≈500 K (Figure 3d), which is sufficiently high to form a stable CNF and results in non-volatile BD. Therefore, the Ag/h-BN/Au devices can only be operated in threshold-type RS regime when the temperature of the CNF is kept low, and they switch to non-volatile regime when the CNF temperature increases significantly (i.e., >500 K).

2.3. Dynamic Characteristics and Cycle-To-Cycle Variability

Finally, we analyze the dynamic characteristics and the cycle-to-cycle variability of the currents driven by the Ag/h-BN/Au devices in threshold mode by calculating the transition rate (TR) for different V_W, which is defined as dI/dt [A/s], and it

© 2021 Wiley-VCH GmbH

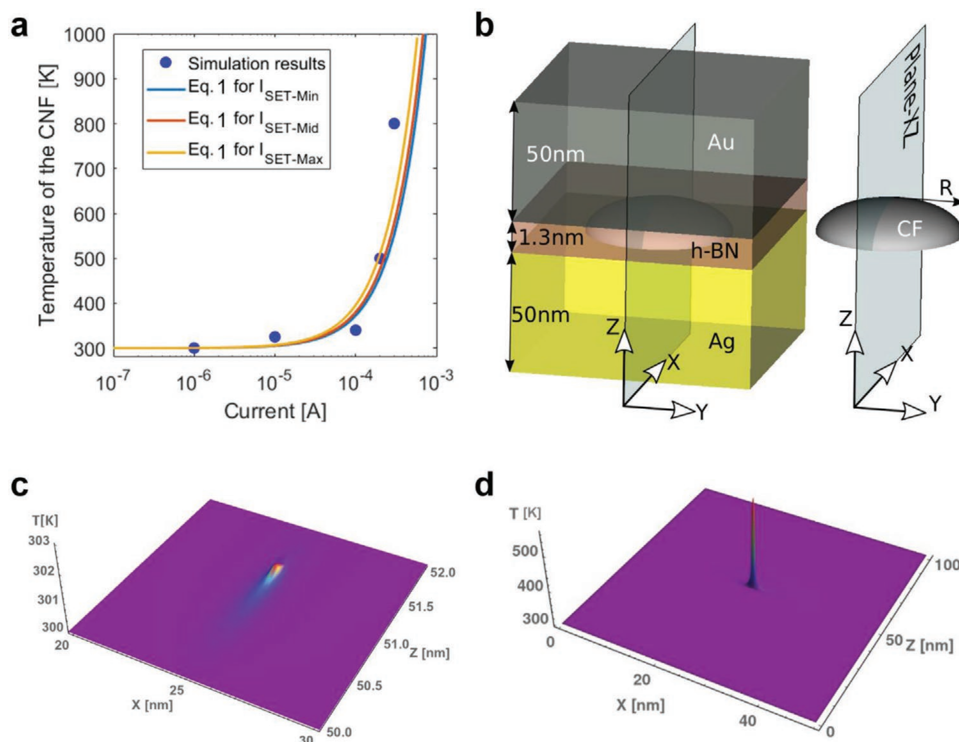

Figure 3. Temperature calculation of the conductive nanofilaments in Au/Ag/CVD-grown h-BN/Au devices. a) Temperature of the CNF as a function of I_{SET}, calculated using Equation (1). High currents in the CNF translate into increase of temperature, which leads to catastrophic failure. b) Simulation domain employed in the analysis performed in 3D heat equation (Equation (2)). c,d) Temperature distribution at the CNF region for I_{CC} = 1 µA and I_{CC} = 200 µA, respectively.

can be extracted from the PVS measurements (Figure 2c,d). Statistically, we observe that TR increases almost two orders of magnitude for the range of V_W used in this study (see scattered symbols in **Figure 4**a). This observation indicates that the CNF formation is driven by ionic motion, which is accelerated at higher electrical fields, as expected.[6,34] Taking into account that in h-BN atoms of N do not move until the melting point of the h-BN,[35] and that B movement leaves behind an N path that is not conductive enough to produce a set transition, most probably the ions being moved during CNF formation are Ag^+ that try to flow toward the cathode (i.e., Au electrode) when a positive bias is applied to the anode (i.e., Ag electrode).[14–15] The time between the onset of T_W and the moment in which the current starts to increase above the noise level (i.e., difference between points 1 and 2 in Figure 2c) is referred as t_{SET}, and it decreases when V_W increases (see Figure 4b). Figure 4b also

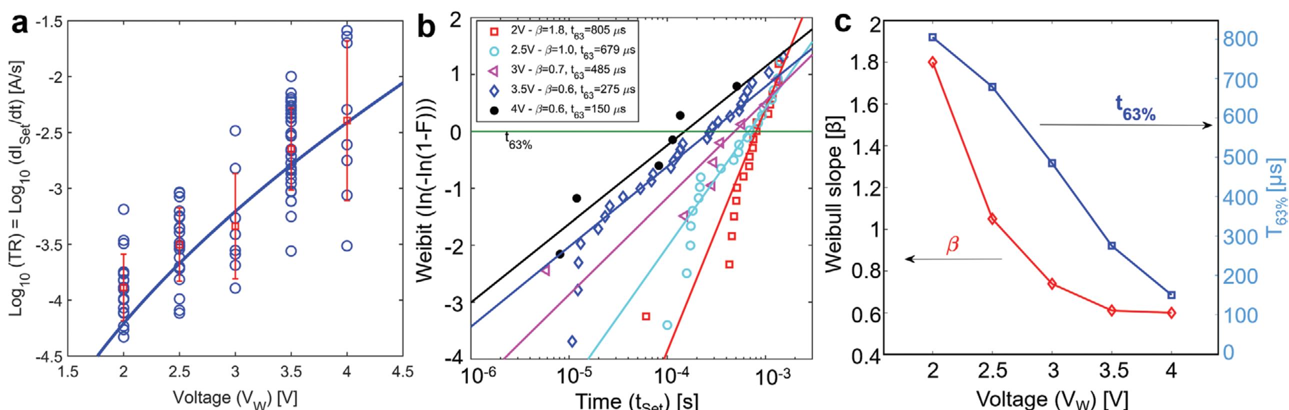

Figure 4. Dynamic characteristics and the cycle-to-cycle variability of the current driven by the Au/Ag/CVD-grown h-BN/Au devices in threshold regime. a) TR for each current transient as a function of the pulse amplitude. b) The distribution of the Time-to-SET follow a Weibull distribution with a clear voltage dependence. c) Extracted trends of β and $t_{63\%}$ are plotted as function of the pulse amplitudes. Both show a clear decreasing trend as the applied voltage increases.

© 2021 Wiley-VCH GmbH

shows that the distribution of t_{SET} for different V_W can be fitted using the Weibull distribution, which is often used to describe weakest-link phenomena (such as dielectric BD in ultra-thin dielectrics).[36] Figure 4c also displays, in a clearer manner, that both, the slope of the Weibull plot (β), which quantifies the variability of t_{SET}, and the value of $t_{63\%}$, which corresponds to the value of t_{SET} at 63% of failed population,[29] decrease with the voltage. Figure 4b,c clearly indicate that the variability of t_{SET} decreases when working at lower V_W, which is an important dynamic characteristic to consider by designers of ANNs made of threshold-type RS devices.

It is very important to emphasize that the state currents and the switching voltages in MIM-like memristors are exposed to cycle-to-cycle and device-to-device variability,[4] which is produced by changes in the width and shape of the CNF filament in each cycle and for each device; consequently, the temperature of the CNF in each cycle and for each device will be different. In operando TEM studies have been used to analyze the size of the CNF in the dielectric with sub-nanometer resolution,[11,37] but even when using such a sophisticated technique the sizes obtained change a lot from one cycle to another; in addition, those studies always use slow constant voltage stresses or ramped voltage stresses to form and disrupt the CNF, which are not consistent with the real operation conditions of the devices —PVS matching the real operation conditions of the devices would be necessary, but TEM does not allow taking images at such high rates. Even if that would be possible, the heat-confinement effect in the thin lamellas for TEM would produce important differences compared to real devices. Therefore, measuring the real size of the CNFs formed using electrical stresses that match real operation conditions and without modifying the boundary conditions remains an unsolved challenge for the entire community working in the field of RS. From the simulation viewpoint, the determination of thermal conductivities for very thin dielectric layers is essential; however, when using novel materials these values are not well established/confirmed. The probable existence of contact resistances between the different materials layers and the lack of accuracy in the knowledge of the thermal and electrical features of the regions were the CNF formation takes place add an important degree of uncertainty in the description of the device thermodynamics. Consequently, the temperature values given in this (and other papers)[38–39] should be understood as qualitative; in this context, the most important conclusion of our investigation is that the operation in threshold regime is strongly related to the CNF temperature.

3. Conclusion

In conclusion, the threshold RS mechanism of 150 nm × 150 nm Ag/CVD grown h-BN/Au devices has been statistically analyzed. We find that the physical mechanisms that promote RS in metal/h-BN/metal are thermally activated since their TR follow the Arrhenius' equation. We have estimated the temperature of the CNFs in Ag/h-BN/Au devices through different simulation approaches, and our calculations show that Ag/h-BN/Au devices can be operated in the threshold-RS regime only when the temperature of the CNF does not surpass a critical limit (of ≈500 K). The used metallic electrodes are also important for the RS behavior in the metal/h-BN/metal devices. If the activation energy of metallic ion reduction mechanisms is low enough, the temperature difference obtained can be sufficient to form a non-volatile CNF that can trigger the BD, and the device stops working in threshold regime. The findings of this study help to understand the performance and reliability of h-BN based RS devices and could also apply to other 2D materials based RS devices.

4. Experimental Section

Deposition of Large-Scale h-BN Stacks: The h-BN stacks are synthesized via CVD by using ammonia borane as precursor and ≈20 µm Cu foil as substrate. During the h-BN growth, The Cu foils are loaded into a CVD-fused quartz tube with a diameter of 5 cm, which is heated to the specified value in the range of 1050–1090 °C, and the total pressure is maintained at 50 Pa. Meanwhile, ammonia borane precursor placed in an Al_2O_3 boat is heated to 70–90 °C by a heating lamp. After the growth, both the heating furnace and heating lamp are quickly cooled down to room temperature.

Fabrication of Scaled Metal/h-BN/Metal Cross-Point Devices: Bottom electrodes consisting of 150 nm × 100 µm × 50 nm (width × length × height) wires connected to 100 µm × 100 µm × 50 nm pads are deposited on a 300 nm SiO_2/Si wafer using electron beam lithography (EBL, Elphy VII from Raith company) integrated in a Supra 55 scanning electron microscope (SEM). Then, a sheet of multilayer h-BN grown by CVD is transferred using the method reported in ref. [15]. Finally, top electrodes with the same shape than the bottom ones (but rotated 90°) are deposited on the h-BN. The material of the top electrode was Ag, and the bottom electrode was Au. The wires of the top and bottom electrodes cross each other, leading to Ag/h-BN/Au devices with sizes of 150 nm × 150 nm. All the metal films are deposited through electron beam evaporator (PVD75, Kurt J. Lesker company).

Physical and Electrical Characterizations of Scaled Metal/h-BN/Metal Devices: The correct layered structure of the h-BN sheets and the effective thickness of the h-BN layers are corroborated in situ via cross-sectional TEM (JEOLJEM-2100). Prior to the TEM characterization, the as-grown h-BN on the Cu substrate is protected with 40 nm Au and 20 nm Ti metal films, and focus ion beam (FIB, model: HELIOS NANOLAB 450S from FEI) is used to obtain thin lamellas. The Ag/h-BN/Au devices are characterized using a Cascade probe station (Model M150) connected to a Keysight B1500A SPA. All the electrical tests in this work have been applied to the top Ag electrode, keeping the Au bottom electrode grounded.

Supporting Information

Supporting Information is available from the Wiley Online Library or from the author.

Acknowledgements

This work has been supported by the Baseline funding scheme of the King Abdullah University of Science and Technology (KAUST) in Saudi Arabia, the Ministry of Science and Technology of China (Grant No. 2018YFE0100800), the National Natural Science Foundation of China (Grants No. 11661131002, 61874075), the Ministry of Finance of China (grant no. SX21400213), the 111 Project from the State Administration of Foreign Experts Affairs of China, the Collaborative Innovation Centre of Suzhou Nano Science & Technology, the Jiangsu Key Laboratory for Carbon-Based Functional Materials & Devices, and the Priority Academic

© 2021 Wiley-VCH GmbH

Program Development of Jiangsu Higher Education Institutions, the MINCyT (Contract Nos. PICT2013/1210, PICT2016/0579, and PME2015-0196), CONICET (Project No. PIP-11220130100077CO), and UTN.BA (Project Nos. PID-UTN EIUTIBA4395TC3, CCUTIBA4764TC, MATUNBA4936, CCUTNBA5182, and CCUTNBA0006615). Y.S. acknowledge support from the European Union (Marie Sklodowska-Curie actions, Grant No. 894840).

Conflict of Interest

The authors declare no conflict of interest.

Data Availability Statement

The data that support the findings of this study are available from the corresponding author upon reasonable request.

Keywords

conductive nano-filaments, hexagonal boron nitride, memristor, temperature calculation, threshold resistive switching

Received: June 15, 2021
Published online:

[1] Q. Xia, J. J. Yang, *Nat. Mater.* **2019**, *18*, 309.
[2] S. Spiga, *Memristive Devices for Brain-Inspired Computing*, Elsevier, New York **2020**.
[3] D. Ielmini, R. Waser, *Resistive Switching: From Fundamentals of Nanoionic Redox Processes to Memristive Device Applications*, John Wiley & Sons, New York **2015**.
[4] M. Lanza, H.-S. P. Wong, E. Pop, D. Ielmini, D. Strukov, B. C. Regan, L. Larcher, M. A. Villena, J. J. Yang, L. Goux, A. Belmonte, Y. Yang, F. M. Puglisi, J. Kang, B. Magyari-Köpe, E. Yalon, A. Kenyon, M. Buckwell, A. Mehonic, A. Shluger, H. Li, T.-H. Hou, B. Hudec, D. Akinwande, R. Ge, S. Ambrogio, J. B. Roldan, E. Miranda, J. Suñe, K. L. Pey, X. Wu, N. Raghavan, E. Wu, W. D. Lu, G. Navarro, W. Zhang, H. Wu, R. Li, A. Holleitner, U. Wurstbauer, M. C. Lemme, M. Liu, S. Long, Q. Liu, H. Lv, A. Padovani, P. Pavan, I. Valov, X. Jing, T. Han, K. Zhu, S. Chen, F. Hui, Y. Shi, *Adv. Electron. Mater.* **2019**, *5*, 1800143.
[5] R. Waser, M. Aono, in *Nanoscience and Technology*, Co-Published With Macmillan Publishers Ltd, New York **2009**, pp. 158–165.
[6] R. Waser, R. Dittmann, G. Staikov, K. Szot, *Adv. Mater.* **2009**, *21*, 2632.
[7] W. Wang, M. Wang, E. Ambrosi, A. Bricalli, M. Laudato, Z. Sun, X. Chen, D. Ielmini, *Nat. Commun.* **2019**, *10*, 81.
[8] B. J. Choi, D. S. Jeong, S. K. Kim, C. Rohde, S. Choi, J. H. Oh, H. J. Kim, C. S. Hwang, K. Szot, R. Waser, B. Reichenberg, S. Tiedke, *J. Appl. Phys.* **2005**, *98*, 033715.
[9] D.-H. Kwon, K. M. Kim, J. H. Jang, J. M. Jeon, M. H. Lee, G. H. Kim, X.-S. Li, G.-S. Park, B. Lee, S. Han, M. Kim, C. S. Hwang, *Nat. Nanotechnol.* **2010**, *5*, 148.
[10] Y. Yang, W. Lu, *Nanoscale* **2013**, *5*, 10076.
[11] Z. Wang, S. Joshi, S. E. Savel'ev, H. Jiang, R. Midya, P. Lin, M. Hu, N. Ge, J. P. Strachan, Z. Li, Q. Wu, M. Barnell, G.-L. Li, H. L. Xin, R. S. Williams, Q. Xia, J. J. Yang, *Nat. Mater.* **2017**, *16*, 101.
[12] S. Chen, M. R. Mahmoodi, Y. Shi, C. Mahata, B. Yuan, X. Liang, C. Wen, F. Hui, D. Akinwande, D. B. Strukov, M. Lanza, *Nat. Electron.* **2020**, *3*, 638.
[13] B. E. A. Saleh, M. C. Teich, *Fundamentals of Photonics*, John Wiley & Sons, New York **2019**.
[14] C. Pan, Y. Ji, N. Xiao, F. Hui, K. Tang, Y. Guo, X. Xie, F. M. Puglisi, L. Larcher, E. Miranda, L. Jiang, Y. Shi, I. Valov, P. C. McIntyre, R. Waser, M. Lanza, *Adv. Funct. Mater.* **2017**, *27*, 1604811.
[15] Y. Shi, X. Liang, B. Yuan, V. Chen, H. Li, F. Hui, Z. Yu, F. Yuan, E. Pop, H.-S. P. Wong, M. Lanza, *Nat. Electron.* **2018**, *1*, 458.
[16] T. Gokmen, Y. Vlasov, *Front. Neurosci.* **2016**, *10*, 333.
[17] R. Midya, Z. Wang, J. Zhang, S. E. Savel'ev, C. Li, M. Rao, M. H. Jang, S. Joshi, H. Jiang, P. Lin, K. Norris, N. Ge, Q. Wu, M. Barnell, Z. Li, H. L. Xin, R. S. Williams, Q. Xia, J. J. Yang, *Adv. Mater.* **2017**, *29*, 1604457.
[18] T. Ohno, T. Hasegawa, T. Tsuruoka, K. Terabe, J. K. Gimzewski, M. Aono, *Nat. Mater.* **2011**, *10*, 591.
[19] G. Milano, M. Luebben, Z. Ma, R. Dunin-Borkowski, L. Boarino, C. F. Pirri, R. Waser, C. Ricciardi, I. Valov, *Nat. Commun.* **2018**, *9*, 5151.
[20] A. Falin, Q. Cai, E. J. G. Santos, D. Scullion, D. Qian, R. Zhang, Z. Yang, S. Huang, K. Watanabe, T. Taniguchi, M. R. Barnett, Y. Chen, R. S. Ruoff, L. H. Li, *Nat. Commun.* **2017**, *8*, 15815.
[21] L. H. Li, J. Cervenka, K. Watanabe, T. Taniguchi, Y. Chen, *ACS Nano* **2014**, *8*, 1457.
[22] Z. Liu, Y. Gong, W. Zhou, L. Ma, J. Yu, J. C. Idrobo, J. Jung, A. H. MacDonald, R. Vajtai, J. Lou, P. M. Ajayan, *Nat. Commun.* **2013**, *4*, 2541.
[23] Q. Cai, D. Scullion, W. Gan, A. Falin, S. Zhang, K. Watanabe, T. Taniguchi, Y. Chen, E. J. G. Santos, L. H. Li, *Sci. Adv.* **2019**, *5*, eaav0129.
[24] F. Palumbo, S. Lombardo, M. Eizenberg, *J. Appl. Phys.* **2014**, *115*, 224101.
[25] F. Palumbo, M. Eizenberg, S. Lombardo, in *2015 IEEE Int. Reliability Physics Symp.*, IEEE, Piscataway, NJ **2015**, pp. 5A.1.1–5A.1.6.
[26] S. Lombardo, J. H. Stathis, B. P. Linder, *Phys. Rev. Lett.* **2003**, *90*, 167601.
[27] R. Pagano, S. Lombardo, F. Palumbo, P. Kirsch, S. A. Krishnan, C. Young, R. Choi, G. Bersuker, J. H. Stathis, *Microelectron. Reliab.* **2008**, *48*, 1759.
[28] F. Palumbo, S. Lombardo, J. H. Stathis, V. Narayanan, F. R. McFeely, J. J. Yurkas, in 2004 IEEE Int. Reliability Physics Symp., Proc., IEEE, Piscataway, NJ **2004**, pp. 122.
[29] S. Lombardo, E. Y. Wu, J. H. Stathis, *J. Appl. Phys.* **2017**, *122*, 085701.
[30] M. Maestro-Izquierdo, M. B. Gonzalez, F. Jimenez-Molinos, E. Moreno, J. B. Roldan, F. Campabadal, *Nanotechnology* **2020**, *31*, 135202.
[31] M. Cazorla, S. Aldana, M. Maestro, M. B. González, F. Campabadal, E. Moreno, F. Jiménez-Molinos, J. B. Roldán, *J. Vac. Sci. Technol., B* **2019**, *37*, 012204.
[32] M. Bocquet, D. Deleruyelle, H. Aziza, C. Muller, J.-M. Portal, T. Cabout, E. Jalaguier, *IEEE Trans. Electron Dev.* **2014**, *61*, 674.
[33] E. Yalon, A. A. Sharma, M. Skowronski, J. A. Bain, D. Ritter, I. V. Karpov, *IEEE Trans. Electron Dev.* **2015**, *62*, 2972.
[34] S. Menzel, M. Waters, A. Marchewka, U. Böttger, R. Dittmann, R. Waser, *Adv. Funct. Mater.* **2011**, *21*, 4487.
[35] F. Pan, S. Gao, C. Chen, C. Song, F. Zeng, *Mater. Sci. Eng., R* **2014**, *83*, 1.
[36] F. L. Aguirre, A. Padovani, A. Ranjan, N. Raghavan, N. Vega, N. Müller, S. Matías Pazos, M. Debray, J. Molina, K. L. Pey, F. Palumbo, in *2019 IEEE Int. Reliability Physics Symp. (IRPS)* **2019**, pp. 1–8, https://doi.org/10.1109/IRPS.2019.8720539.
[37] Y. Yang, Y. Takahashi, A. Tsurumaki-Fukuchi, M. Arita, M. Moors, M. Buckwell, A. Mehonic, A. J. Kenyon, *J. Electroceram.* **2017**, *39*, 73.
[38] A. J. Lohn, P. R. Mickel, M. J. Marinella, *J. Appl. Phys.* **2014**, *115*, 234507.
[39] S. Kwon, S. Jang, J.-W. Choi, S. Choi, S. Jang, T.-W. Kim, G. Wang, *Nano Lett.* **2017**, *17*, 7462.

 © 2021 Wiley-VCH GmbH